JEE Journal of Ecological Engineering

Journal of Ecological Engineering 2021, 22(10), 109–120
https://doi.org/10.12911/22998993/142122
ISSN 2299–8993, License CC-BY 4.0

Received: 2021.08.15
Accepted: 2021.09.14
Published: 2021.10.01

Soft Ion Divalent Metals toward Adsorption on Zn/Al-POM Layered Double Hydroxide

Luna Silaen[1], Elfita[2], Risfidian Mohadi[3], Normah[4], Novie Juleanti[4], Neza Rahayu Palapa[4], Aldes Lesbani[1,4*]

[1] Graduate School, Faculty of Mathematics and Natural Sciences, Sriwijaya University, Jl. Padang Selasa No. 524 Ilir Barat 1, Palembang-South Sumatra, Indonesia

[2] Department of Chemistry, Faculty of Mathematics and Natural Sciences, Sriwijaya University, Jl. Palembang-Prabumulih, Km. 32, Ogan Ilir, South Sumatra, Indonesia

[3] Department of Environmental Science, Graduate School, Sriwijaya University, Jl. Padang Selasa No. 524 Ilir Barat 1, Palembang-South Sumatra, Indonesia

[4] Research Center of Inorganic Materials and Coordination Complexes, Faculty of Mathematics and Natural Sciences, Sriwijaya University, Jl. Palembang Prabumulih Km.32 Ogan Ilir 30662, Indonesia

* Corresponding author's e-mail: aldeslesbani@pps.unsri.ac.id

ABSTRACT

Development of Zn/Al layered double hydroxide by intercalation using polyoxometalate (POM) $K_4[\alpha\text{-}SiW_{12}O_{40}]$ to Zn/Al-POM was investigated. The success of the modification is evidenced by the XRD, FT-IR, and BET characterization data. XRD characterization showed an increase in the interlayer distance from 8.59 Å in Zn/Al LDHs to 10.26 Å in Zn/Al-POM. This success is also supported by the FT-IR data with the appearance of vibrations around 779–979 cm^{-1} which indicates the vibration of the polyoxometalate compound in Zn/Al-POM. Other supporting data in the form of BET also prove an increase in surface area from 1.968 m^2/g in Zn/Al LDHs to 14.042 m^2/g Zn/Al-POM. The ability of Zn/Al-POM as an adsorbent is proven through several parameters such as kinetics, isotherm, thermodynamics, and regeneration for Cd^{2+}, Pb^{2+}, Ni^{2+}, and Co^{2+}. Adsorption kinetics showed that Zn/Al-POM was more likely to follow the pseudo-second-order adsorption kinetics model for Cd^{2+}, Pb^{2+}, Ni^{2+}, and Co^{2+}. The results of determining the adsorption isotherm parameters of Zn/Al-POM tend to follow the Freundlich isotherm model with a maximum adsorption capacity of 74.13 mg/g on Pb^{2+}. The regeneration process showed that Zn/Al-POM was more resistant than Zn/Al LDHs up to 3 cycles. It was proven that Zn/Al-POM was able to survive in the last cycle up to 69.19% on Ni^{2+}.

Keywords: soft divalent metal ions, adsorption, polyoxometalate, regeneration

INTRODUCTION

The impact and risks of pollutants from heavy metal ions are currently faced all over the world because metal ions have very dangerous, carcinogenic properties and cause environmental damage [Chakraborty et al., 2020]. The heavy metal pollution in liquid waste that is directly discharged into the environment comes from various industries, such as mining, chemical, paint, paper, battery manufacturing, textiles, etc. [Chakraborty et al., 2020; Zhao et al., 2020]. Because heavy metals cannot be recycled (they are non-degradable) and accumulate in living organisms, they pose a long-term risk to humans and ecosystems [Wang and Zhang, 2020]. In the environment, heavy metals have a low toxicity level of around 1.0–10.0 mg/L, Therefore, reducing the heavy metal levels from wastewater in the environment has become a major, serious matter, and an urgent task [Chakraborty et al., 2020].

Tchounwou et al., [2012] reported that metals such as cobalt (Co), lead (Pb), cadmium (Cd), and nickel (Ni) have a non-biological functions in

the body and are considered non-essential metals. Thus, metal ions are stable and if they enter the body, they cannot be metabolized [Taiwo and Chinyere, 2016]. Higher and excessive concentrations of Co^{2+} in sewage can cause depression, diarrhea, paralysis, dermatitis, lung irritation, and even death. Therefore, these metals should be removed to prevent extensive capillary damage, liver and kidney damage as well as irritation of the central nervous system [Kushwaha et al., 2017]. Nickel is an essential and widely used alloying element in high-temperature-resistant superalloys and heat, oxidation, and corrosion-resistant irons and steels. Nickel metal in the environment can damage the ecosystem. Ni, when exposed to the human body in small amounts, causes vomiting, chest pain, and shortness of breath, while in large quantities it can be fatal [Chen and Wang, 2006]. Pb^{2+} is a metal that has a high level of toxicity and tends to accumulate in living organisms and will not be metabolized. Through ingestion of food and water, Pb in inorganic form can cause disturbances, especially in the peripheral nervous system and hematopoietic system, kidneys, while organic lead will affect the work of the central nervous system [Moyo et al., 2013]. In some papers it was identified that Cd^{2+} is produced from the open-pit coal mining process, with serious consequences [Wang et al., 2020]. It has been reported [Hoyos-Sánchez et al., 2017] that cadmium poisoning can cause kidney, bone, and lung damage.

Researchers have carried out decontamination of the environmental water contaminated by heavy metals using such methods as chemical precipitation, filtration, electrochemistry, coagulation-flocculation, oxidation, ion exchange, and adsorption [Cocheci et al., 2010; Ali et al., 2012; Mohamed et al., 2019; Castro-Castro et al., 2020; Normah et al., 2021] The adsorption method is preferred due to its simplicity, low cost, the ease of operation , the flexibility of the design and the choice of adsorbent, as well as environmental friendliness [Oktriyanti et al., 2019; Forghani et al., 2020; Silaen et al., 2020]. On the basis of various works of literature, different types of adsorbents have been applied to reduce the levels of heavy metals contained in wastewater, including the adsorbents that have porous or layered characteristics, such as bentonite, activated carbon, kaolin, and layered double hydroxides (LDHs) [Wahab et al., 2019; Chai et al., 2020; Zhang et al., 2020a].

LDHs are a kind of anionic mineral with a positively charged layer (+) and negatively charged ions (-) or anions in the interlayer [Zhang et al., 2019]. LDHs are mineral-like hydrotalcite, which have a unique characterization [Lin et al., 2018]. The general form of LDHs written as $[M^{2+}1\text{-}xM^{3+}x\ (OH)_2]^{x+}\ [A^{n-}_{x/n}.mH_2O]$ where M^{2+} (divalent metal ion) and M^{3+} (trivalent metal ion). A^{n-} indicates organic or inorganic anions with n- valence [Tang et al., 2020]. Divalent and trivalent metals generally come from groups 2 and 3 and transition metal ions are periodic elements [Zhang et al., 2020b]. The anions in the LDHs interlayer are interchangeable depending on the synthetic conditions as well as the LDHs application [Silaen et al., 2021]. The interlayer of LDHs contains many anions (generally nitrate, sulfate, and carbonate). Thus, many researchers have succeeded in applying various larger anions that can replace them. These anions include amino acids, citric acid, malic, and polyoxometalate [Lin et al., 2018; Palaopa et al., 2021a] Polyoxometalate compounds are inorganic metal-oxygen cluster compounds [Silaen et al., 2021]. Polyoxometallic types such as $K_3[\alpha\text{-}PW_{12}O_{40}]$ and $K_4[\alpha\text{-}SiW_{12}O_{40}]$ have been widely used as intercalant for anion exchange in the LDHs interlayer [Oktriyanti et al., 2020]. Keggin ion $[\alpha\text{-}SiW_{12}O_{40}]^{4-}$ was intercalated as an intercalator to Zn/Cr LDHs. The results of the synthesis are used to remove iron(II) metal ions. On the basis of the research of [Lesbani et al., 2020] synthesized Ni/Al LDHs were intercalated with ion $[\alpha\text{-}SiW_{12}O_{40}]^{4-}$ and used to remove iron(II). All these results indicate that LDHs after intercalation with polyoxometalates have unique properties and characteristics.

Tchounwou et al., [2012] used a metal with border types and soft metal; this is because borderline (Cd) and soft metal (Pb, Ni and Co) are non-essential and include heavy metals with a high level of toxicity, while hard metals are usually essential and non-toxic. Based on Alfarra et al., [2004] that the Pearson acid-base concept states HSAB is widely used in chemistry for explaining the stability of compounds, reaction mechanisms, and pathways. Essentially, the theory states that soft acids react faster and form stronger bonds with soft bases, whereas hard acids react faster and form stronger bonds with hard bases, all other factors being equal, or "hard likes hard, soft likes soft". The HSAB concept also explained that the interaction between a soft

metal ion, such as Cd^{2+} with LDH is weak but with Pb^{2+}, Ni^{2+}, and Co^{2+} is higher than LDH.

In research, the Keggin ion $[\alpha\text{-}SiW_{12}O_{40}]^{4-}$ was intercalated to Zn/Al LDHs to form Zn/Al-POM. The synthesized adsorbents, namely Zn/Al LDHs and the intercalated Zn/Al-POM were analyzed using X-Ray Diffraction (XRD), FTIR spectrophotometer (FTIR), and nitrogen adsorption-desorption apparatus (BET analysis). Then, the material was used as an adsorbent of Co^{2+}, Cd^{2+}, Ni^{2+}, and Pb^{2+} from wastewater. The selection of Cd^{2+}, Ni^{2+}, Pb^{2+}, Co^{2+} metals was based on the differences in adsorbent properties, where Cd^{2+} metal is borderline and Pb^{2+}, Ni^{2+} and Co^{2+} are soft while adsorbents (LDHs) are hard. On the basis of the classification of adsorbate, it can be proven that in the adsorption process there is a role for the HSAB theory. The interaction of an adsorbent and adsorbate tends to affect the adsorption capacity (Qmax). The removal of metal in the aqueous phase was carried out by influencing variations in adsorption, including the effect of the contact time of the adsorbent and adsorbate, the initial concentration of each adsorbate and the temperature used during the adsorption process of Zn/Al POM and LDHs. The ability of the synthesized product to carry out the regeneration process for metal adsorption was studied.

MATERIAL AND METHODS

The chemicals used were pre-analytical quality chemicals, such as zinc nitrate ($Zn(NO_3)_2$ $6H_2O$), aluminum nitrate ($Al(NO_3)_3\cdot$ $9H_2O$), nickel (II) nitrate ($Ni(NO_3)_2$ $6H_2O$), cobalt (II) nitrate ($Co(NO_3)_2$ $6H_2O$), chromium (III) nitrate ($Cr(NO_3)_3$ $9H_2O$), cadmium chloride ($CdCl_2$), lead (II) chloride ($PbCl_2$), sodium hydroxide (NaOH), sodium carbonate (Na_2CO_3), nitric acid (HNO_3), sodium chloride (NaCl), potassium chloride (KCl), hydrochloric acid (HCl) and distilled water, 1,10-phenanthroline ($C_{12}H_8N_2\cdot H_2O$), acetone (CH_3COCH_3), acetate buffer solution (CH_3COOH-CH_3COONa), hydroxylammonium chloride ($NH_2OH.HCl$) and Sodium Ethylene Diamine Tetra Acetate (Na.EDTA). The tools used in this research include standard laboratory glassware. Other equipment includes a magnetic stirrer, thermometer, hotplate, oven, XRD device (Rigaku Mini Flex 600), FT-IR spectrophotometer (Shimadzu Prestige-21), BET adsorption-desorption apparatus (ASAP 2020), and UV-Vis spectrophotometer (Biobase BK)-UV1800 PC.

Zn/Al LDHs synthesis

Zn/Al LDHs were synthesized at pH 10 with the coprecipitation method [Marques et al., 2020]. As much as 10 mL of 0.75 M $Zn(NO_3)_2\cdot 6H_2O$ solution and 10 mL of 0.25 M $Al(NO_3)_3\cdot 9H_2O$ solution were added slowly to 10 mL NaOH 2 M and stirred at 60°C for 4 hours to obtain a white crystalline solid. The resulting solid was then dried at 100°C for 24 hours. After obtaining Zn/Al LDHs, it was characterized by XRD, FT-IR spectrophotometer and BET surface area analysis.

Polyoxometallate $K_4[\alpha\text{-}SiW_{12}O_{40}]\cdot mH_2O$ synthesis

The synthesis of the polyoxometalate compound $K_4[\alpha\text{-}SiW_{12}O_{40}]\cdot mH_2O$ was carried out using solution A and solution B. Solution A consisted of 11 g of sodium metasilicate dissolved in 100 mL of water. Solution B was 182 g of sodium tungstate dissolved in 300 mL of hot water. Next, solution B was slowly dripped with 165 mL of 4M HCl to avoid the formation of a precipitate. Then, solution A and solution B were mixed and 50 mL of 4M HCl was added. The pH of the mixture was adjusted around pH 6 and then kept for 1 hour at 90°C. After that, the mixture was allowed to stand at room temperature and 50 g of KCl was added until a white precipitate was obtained in the form of $K_4[\alpha\text{-}SiW_{12}O_{40}].mH_2O$ (POM). Characterization of POM compounds was carried out using XRD and FT-IR analysis.

Zn/Al-POM synthesis

The LDHs modification process uses polyoxometalate (POM) compound $K_4[\alpha\text{-}SiW_{12}O_{40}]\cdot mH_2O$ through the intercalation process. The intercalation process was carried out by an ion-exchange reaction with a ratio of the weight of layered double hydroxide: weight of polyoxometalate $K_4[\alpha\text{-}SiW_{12}O_{40}]\cdot mH_2O$ (1:15). The intercalation process was carried out by making 15 grams of POM solution with 50 mL of distilled water and 1 gram of LDHs solution B with 50 mL of distilled water added. Solution B was mixed dropwise into solution A under the condition that it was given N_2 gas and allowed to stand for 24 hours. This

suspension is dried at room temperature. The analysis of Zn/Al-POM was performed using XRD and FT-IR spectrophotometer and BET surface area analysis.

Adsorption Experiment

The effect of the adsorption contact time of Zn/Al LDHs and Zn/Al-POM was determined by varying the contact time of 0, 5, 10, 15, 20, 30, 50, 70, 90, 120, 150 and 180 minutes. A total of 0.02 g of adsorbent was put into a 100 mL Erlenmeyer containing 20 mL of each solution of Co^{2+} ions 25 mg/L, Cd^{2+} 0.5 mg/L, Ni^{2+} 30 mg/L, and Pb^{2+} 20 mg/L. After the stirring was complete, the adsorbent and the remaining metal ions were separated by filtration. The filtrate of metal ions Cd^{2+}, Pb^{2+}, Ni^{2+}, and Co^{2+} and were complexed with 1,10-phenanthroline, respectively. The metal ion complexing process was carried out to form stable metal ion species. The results of the complexing were measured for absorbance using a UV-Vis spectrophotometer.

Determination of isotherm and adsorption thermodynamics of metal ions Cd^{2+}, Pb^{2+}, Ni^{2+}, and Co^{2+} was carried out through a series of experiments by varying the concentration of metal ions Cd^{2+}, Pb^{2+}, Ni^{2+}, and Co^{2+} and adsorption temperature. A total of 0.02 g of Zn/Al LDHs and Zn/Al-POM were mixed, each in 20 mL of metal ion solution Cd^{2+}, Pb^{2+}, Ni^{2+}, and Co^{2+} and stirred for 50 minutes. Each variation of Co^{2+} concentration was (10, 15, 20, 25 and 30) mg/L, Cd^{2+}(5, 10, 15, 20 and 25) mg/L, Ni^{2+} (10 , 15, 20, 25 and 30) mg/L while for Pb^{2+} (25, 30, 35, 40 and 45) mg/L it was carried out at various temperatures, namely (30°C, 40°C, 50°C, and 60°C). The mixture was then filtered; afterwards, the filtrate was complexed and then measured using a UV-Vis spectrophotometer to determine the concentration of residual metal after the adsorption process.

RESULT AND DISSCUSION

The synthesized materials, i.e. Zn/Al LDHs and Zn/Al-POM were characterized using XRD. The diffractogram pattern of Zn/Al LDHs, Zn/Al LDHs intercalated with $[\alpha\text{-}SiW_{12}O_{40}]^{-4}$ is shown in Figure 1. Figure 1 (a) shows the pattern of Zn/Al LDHs material which has peaked. Diffraction with LDHs characteristics, such as hydrotalcite according to JCPDS No.38–0486 [Zhang et al., 2013] with diffraction fields (003), (006), (012), (015), (110), (018) and (113) [31].

Zn/Al LDHs have an XRD pattern with characteristic sharp and symmetrical peaks at an angle of 2θ; this indicates that LDHs have a layered structure with high crystallinity. The distance between layers, d for an angle of 2θ 10.29° (003) Zn/Al LDHs plane of 8.59Å is a characteristic of the nitrate anion in the interlayer [Mamat et al., 2018]. Zn/Al LDHs is intercalated with $[\alpha\text{-}SiW_{12}O_{40}]^{-4}$ ion to form Zn/Al-POM. The diffractogram pattern of the Zn/Al-POM material shown in Figure 1 (b) appears in the diffraction planes (003), (006), (012), (110), and (018) which signify Zn/Al LDHs that remains. Diffraction at d for an angle of 2θ 8.53° (003) reaches 10.26 Å. The distance between layers increased by 11.76 Å after the intercalation process.

Adsorption-desorption of N_2 on Zn/Al LDHs and Zn/Al-POM materials are shown in Figure 2. The profiles in both materials show the hysteresis loop. The adsorption curve has a different shape from the desorption curve because of the pore and irregular shape of the structure. Figure 2 shows the N_2 desorption adsorption pattern which refers to type IV, namely hysteresis which shows mesoporous size [Moller and Pich]. Figure 2 is supported by the data shown in Table 1. The physical properties of Zn/Al-POM have a larger surface area than Zn/Al LDHs. The insertion of $[\alpha\text{-}SiW_{12}O_{40}]^{-4}$ ion in Zn/Al LDHs causes the pore diameter of Zn/Al-POM to be smaller than that of Zn/Al LDHs due to the irregular shape of Zn/Al-POM after intercalation.

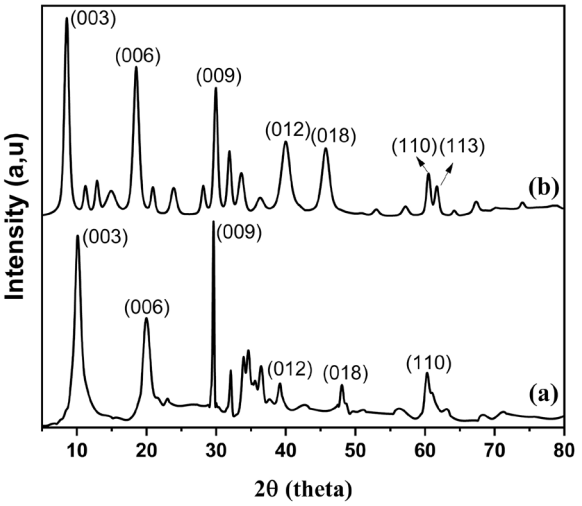

Figure 1. Diffractogram of Zn/Al LDHs (a), Zn/Al-POM (b)

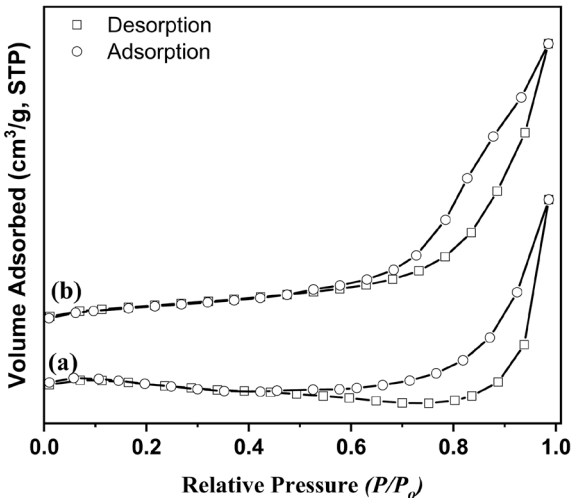

Figure 2. BET isotherm pattern of Zn/Al LDHs (a), Zn/Al-POM (b)

Figure 3 shows the spectrum of Zn/Al LDHs and Zn/Al-POM FTIR materials. Figure 3 (a) shows the vibrational peak of Zn/Al LDHs appears at a wave number of 3456 cm^{-1} (υ-OH stretching) which is bound to the hydroxyl group of the LDHs layer and H_2O molecules in the interlayer, the peak of the vibration is at 1635 cm^{-1} (υ -OH bending), 1381 cm^{-1} (υ NO) which is preoccupied with nitrate anions, and peaks at lower numbers below 1000 cm^{-1} with metal-oxygen (O-M-O, M-O, M-O-M) [Mamat et al., 2018]. Zn/Al-POM has an FTIR spectrum, as shown in Figure 3 (b). There is a vibration peak of Zn/Al-POM at 887 cm^{-1}, 1381 cm^{-1}, 1635 cm^{-1}, 3448 cm^{-1}. The vibration peak at 1381 cm^{-1} increased sharply due to the process of exchanging nitrate ions with $[\alpha\text{-}SiW_{12}O_{40}]^{-4}$ ions. The $[\alpha\text{-}SiW_{12}O_{40}]^{-4}$ ion is not

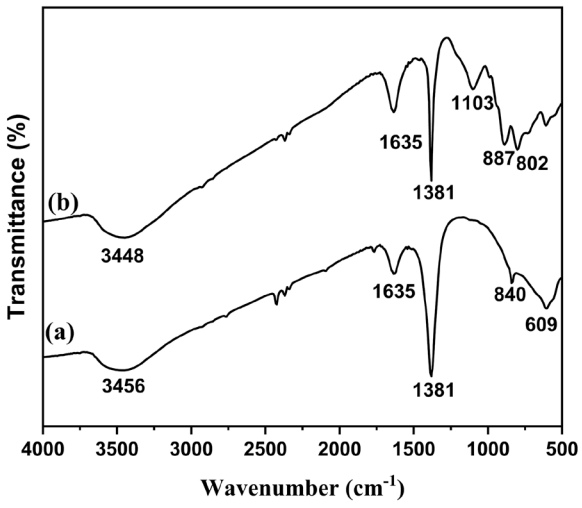

Figure 3. FT-IR spectra of Zn/Al LDHs (a), Zn/Al-POM (b)

Table 1. BET surface area and pore characteristics

Material	S_{Area} (m^2/g)	S_{pore} (nm), BJH	V_{pore} (cm^3/g), BJH
Zn/Al LDHs	1.968	27.687	0.006
Zn/Al-POM	14.042	17.459	0.055

completely exchanged, because it is larger than the nitrate ion. The presence of a unique vibration in the range of 779–979 cm^{-1} indicates that the $[\alpha\text{-}SiW_{12}O_{40}]^{-4}$ ion is in the LDHs interlayer, so that this intercalation process was successfully carried out.

The measurement of pH pzc was carried out to determine the state in which the Zn-Al and Zn/Al-POM materials were zero or uncharged [Lesbani et al., 2018; Sharifpour et al., 2019]. The pH pzc of Zn/Al LDHs and Zn/Al-POM are shown in Figure 4. The Zn/Al LDHs material has a cut-off point at pH 4.3 and Zn/Al-POM at pH 5.8. Thus, at the point of intersection is the pH pzc of Zn/Al LDHs and Zn/Al-POM. The material will be positively charged if the pH of the material is below pH pzc with a large amount of H^+, whereas if the material is above pH pzc, then the material is negatively charged with a dominant number of OH^- ions. Furthermore, before the adsorption process was carried out, the pH was first adjusted according to the pH pzc of each material [Silaen et al., 2021].

The adsorption isotherm was carried out at a constant concentration by varying the adsorption temperature. The adsorption isotherm model determined was Langmuir and Freundlich. According to [Cai et al., 2012], the determination of the adsorption isotherm model is based on the R^2 which is closer to 1. Figure 5 shows the tendency of the R^2 value of the Cd^{2+}, Pb^{2+}, Ni^{2+}, and Co^{2+} adsorption processes in the Freundlich isotherm model to be closer to 1, this is also reinforced by the data presented in Table 2.

On the basis of the [Onder et al., 2020] research, the tendency of the Freundlich isotherm model shows that adsorption occurs in multilayers on heterogeneous surfaces. In addition to the isotherm model, the maximum capacity of the adsorption process is also presented in Table 2. The use of Zn/Al LDHs and Zn/Al-POM as adsorbents Cd^{2+}, Pb^{2+}, Ni^{2+}, and Co^{2+} resulted in different adsorption capacities in each process. The Cd adsorption process showed the smallest maximum adsorption capacity of 0.95 for Zn/Al LDHs and 0.98 for Zn/Al-POM

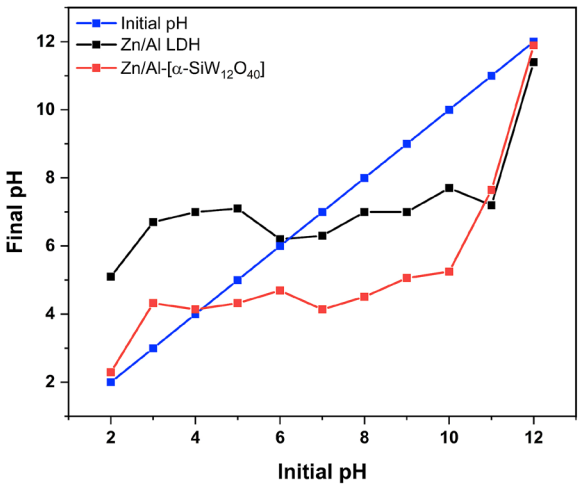

Figure 4. pH PZC analysis of Zn/Al LDHs and Zn/Al-POM

The small value of the maximum adsorption capacity of Cd^{2+} tends to be influenced by the characteristics of the classification of Cd^{2+} as a soft acid (Table 3). The difference in the properties with the adsorbents which are included in the classification of hard acids causes the interaction between the adsorbent and adsorbate to tend to be weak and chemical interactions are difficult to fulfill. The characteristics of these differences have been confirmed by [Alfarra et al., 2004] who stated that Lewis acids/bases in the HSAB principle tend to interact according to "soft likes soft, hard likes hard". Table 3 confirms that the Qmax of Pb^{2+} using Zn/Al-POM reached 74.13 mg/g, Ni^{2+} 55.56 mg/g and Co^{2+} 43.86 mg/g. On the basis of Table 3, Pb^{2+}, Ni^{2+}, and Co^{2+} are classified as acids on the borderline, where these characteristics are close to the adsorbents which are hard acids, so that the adsorbent and adsorbate will be easier to interact. This condition proves that the use of metal ions with different classifications will affect the maximum capacity achieved. On the other hand, the tendency of the Freundlich isotherm model, which is more dominant in the overall adsorption process supports this theory, where the metal ion adsorption process will interact more easily with the adsorbents that have the same classification.

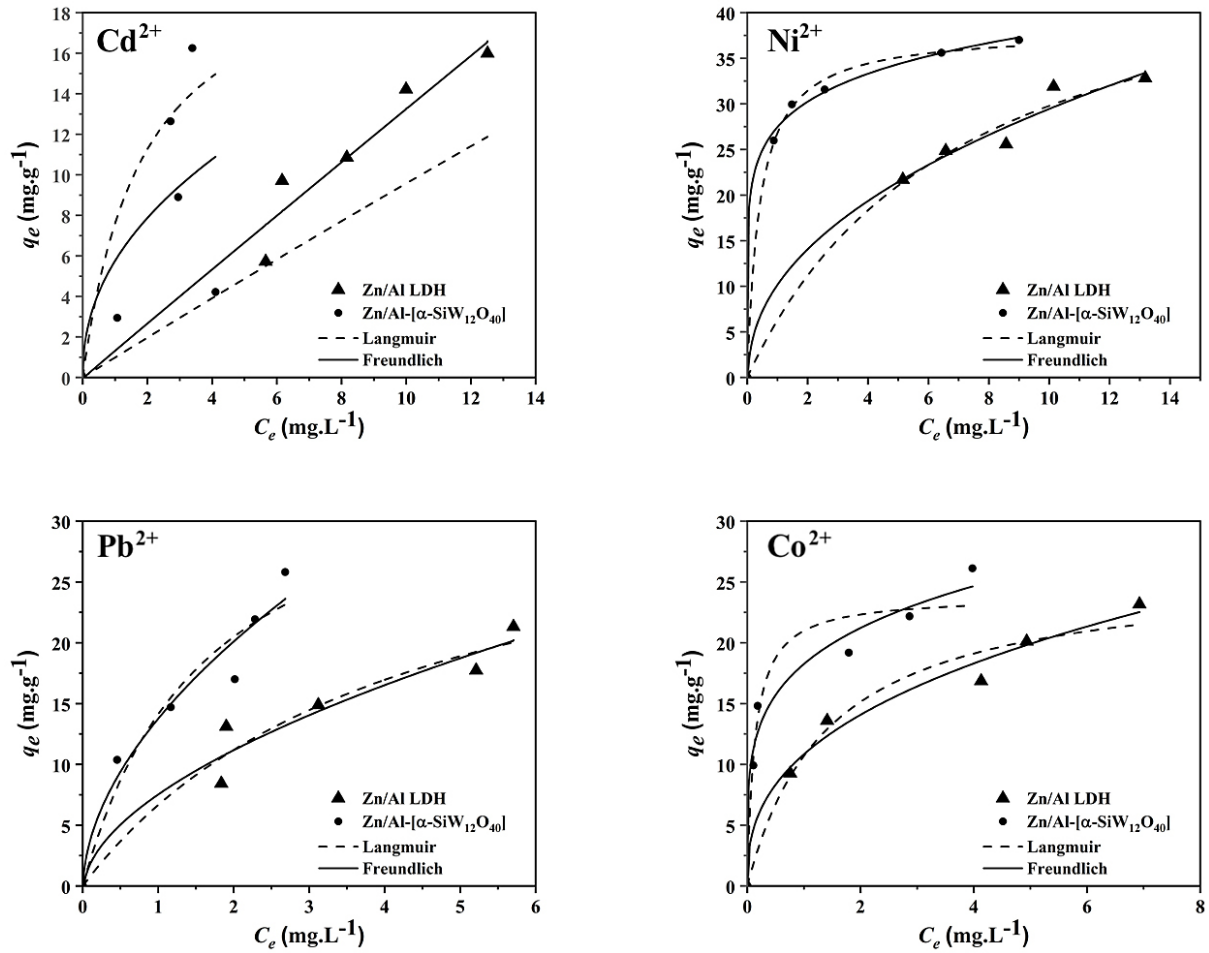

Figure 5. Adsorption isotherm model of (Cd, Ni, Pb, and Co)$^{2+}$ using Zn/Al LDHs and Zn/Al-POM

Table 2. Isotherm model for removal of Cd^{2+}, Pb^{2+}, Ni^{2+}, and Co^{2+}

Adsorbent	Isoterm Model	Adsorption Constant	Metals			
			Cd^{2+}	Ni^{2+}	Pb^{2+}	Co^{2+}
Zn/Al LDHs	Langmuir	Qmax	0.95	46.51	46.95	40.00
		kL	0.80	0.07	0.20	0.23
		R^2	0.94	0.98	0.99	0.98
	Freundlich	n	0.67	1.46	2.49	1.65
		kF	3.74	3.97	12.38	8.00
		R^2	0.99	0.99	0.95	0.99
Zn/Al-POM	Langmuir	Qmax	0.98	55.56	74.13	43.86
		kL	4.69	0.17	0.03	0.11
		R^2	0.74	0.95	0.99	0.99
	Freundlich	n	0.86	1.39	2.80	1.46
		kF	5.10	8.34	7.70	4.87
		R^2	0.99	0.98	0.97	0.99

Furthermore, the thermodynamic parameters presented in Table 4 were determined. The thermodynamic parameters determined in this case are enthalpy (ΔH), entropy (ΔS) and Gibbs free energy (ΔG). Overall, the enthalpy of the adsorption process (Cd, Ni, Pb, and Co)$^{2+}$ resulted in positive values in the range of 28–43 kJ/mol. On the basis of the research of Palapa et al. (2021) [Palapa et al., 2020], the positive enthalpy value confirms that the adsorption is endothermic [Palapa et al., 2021]. Enthalpy which is in the range of 5–40 kJ/mol indicates that the adsorption process occurs by physisorption. The overall enthalpy range below 40 indicates that the adsorption process occurs by physisorption [Juleanti et al., 2021]. The enthalpy value tends to be small because 1 mole of adsorbent does not accommodate 1 mole of the adsorbate. On the basis of the value of Qmax, the adsorption process tends to take place by chemisorption, with chemical interactions that play a role in the adsorption process, causing 1 mole of adsorbent not ideally to bind 1 mole of adsorbate.

Entropy expresses the degree of disorder, where the adsorption process Cd^{2+}, Pb^{2+}, Ni^{2+}, and Co^{2+} with Zn/Al LDHs and Zn/Al-POM produces a positive value (0.08–0.15 J/mol.K). This positive result assumes that there is an interaction between the solid-liquid surface of the adsorbent and the adsorbate during the adsorption process [Normah et al., 2021]. Table 4 also shows negative values for the Gibbs free energy of the entire adsorption process using Zn/Al LDHs and Zn/Al-POM. According to [Siregar et al., 2021], a negative value for the Δ G confirmed that the adsorption process tends to occur spontaneously.

The adsorption process with the effect of adsorption contact time is shown in Figure 6. Figure 6 shows the adsorption of Cd^{2+}, Pb^{2+}, Ni^{2+}, and Co^{2+} on Zn/Al LDHs and Zn/Al-POM reached equilibrium at an adsorption time of 60 min. The adsorption data on the effect of adsorption time

Table 3. The HSAB principle by [Hamisu et al., 2020], classification of hard and soft acids bases

Classification	Hard	Borderline	Soft
Acids	Na^+, H^+, K^+, Li^+, Cs^+, Rb^+, Be^{2+}, Ca^{2+}, Mg^{2+}, Sr^{2+}, Al^{3+}, Sc^{3+}, Ga^{3+}, In^{3+}, La^{3+}, Gd^{3+}, Lu^{3+}, Y^{3+}, Ti^{3+}, V^{3+}, Cr^{3+}, Fe^{3+}, As^{3+}, Sn^{3+}, Co^{3+}, Ni^{3+}, Mo^{3+}, Ru^{3+}, Tb^{3+}, Eu^{3+}, Sm^{3+}, Si^{4+}, Ti^{4+}, Zr^{4+}, Th^{4+}, U^{4+}, Pu^{4+}, Hf^{4+}, WO^{4+}	Cu^{2+}, Sb^{3+}, Fe^{2+}, Zn^{2+}, Co^{2+}, Ru^{2+}, Ni^{2+}, Pb^{2+}, Bi^{3+}, Sn^{2+}, Rh^{3+}, Ir^{3+}, Os^{2+}, Mn^{2+}, Fe^{3+}, Sc^{2+}, Ti^{2+}, V^{2+}, Cr^{3+}, Ge^{2+}, Y^{2+}, Zr^{2+}, Nb^{2+}, Mo^{2+}, W^{2+}, Mn^{3+}	Cu^+, Ir^+, Ag^+, Te^{4+}, Au^+, Hg^+, Tl^+, Cd^{2+}, Co^+, Pd^{2+}, Pt^{2+}, Hg^{2+}, Pt^{4+}, Rh^+, Rh^{2+}, Pd^{2+}, Cd^{2+}, Ag^{2+}, Hf^{2+}, Tl^{3+}, $Tl(CH_3)_3$, BH_3, $Ga(CH_3)_3$ $GaCl_3$, GaI_3, $InCl_3$, Metal atoms (M_0), Bulk metals
Bases	BDC, BDC-NH2, BDC-Br, DOBDC, 1,3-BDC, TMBDC, BTC, NDC, BTB, [1,1':3',1''-terphenyl]-4,4'',5'- tricarboxylate, 1,3,5-tris(3,5- dicarboxylphenylethynyl)-benzene, TATB, BPT, HETT, N3-BTB, TCPP, BPBTTBA, DCPP,TMBDI, TMQPTC, Me3-MPBA, BDCPPI, 1,3-ADC, FcphSO3, py-PTP, BTBA, OX, MTBC, succinate, BPTA,	Aniline, pyridine, 3,4- PYDC, bIM, PZDC, DCBPY, nIM, methionine, ICA, histidine, FTZB, BTDC, AB, BPPCOO, L16	DABCO, 4,4'-BPY, BBTA, BTDD, 4-ABPT, MIM, benzene-1,3,5-triyltriisonicotinate, DCIM, BTT, BPBA, F-BPBA, BTP, BPEE, BPE, Adenine, HMTA

Table 4. Thermodynamic parameters for removal of Cd^{2+}, Pb^{2+}, Ni^{2+}, and Co^{2+}

Adsorbate	T (K)	Zn/Al LDHs				Zn/Al-POM			
		Qe	Δ H kJ/mol	Δ S J/mol.K	Δ G kJ/mol	Qe	Δ H kJ/mol	Δ S J/mol.K	Δ G kJ/mol
Cd^{2+}	303	3.05	28.13	0.10	-0.89	3.66	20.10	0.07	-2.09
	313	3.40			-1.85	3.78			-2.82
	323	3.86			-2.81	4.00			-3.55
	333	4.09			-3.76	4.31			-4.28
Ni^{2+}	303	1.26	30.18	0.11	-2.52	9.01	28.36	0.11	-4.08
	313	3.00			-3.60	9.53			-5.15
	323	4.39			-4.68	9.90			-6.22
	333	6.63			-5.76	10.08			-7.29
Pb^{2+}	303	17.21	24.11	0.08	-1.43	22.13	51.28	0.18	-3.52
	313	18.86			-2.27	23.35			-5.33
	323	20.43			-3.12	24.82			-7.14
	333	21.71			-3.96	25.98			-8.94
Co^{2+}	303	7.20	42.43	0.15	-2.10	8.38	79.54	0.27	-3.31
	313	7.89			-3.57	8.84			-6.04
	323	8.46			-5.04	9.49			-8.78
	333	9.26			-6.51	9.92			-11.51

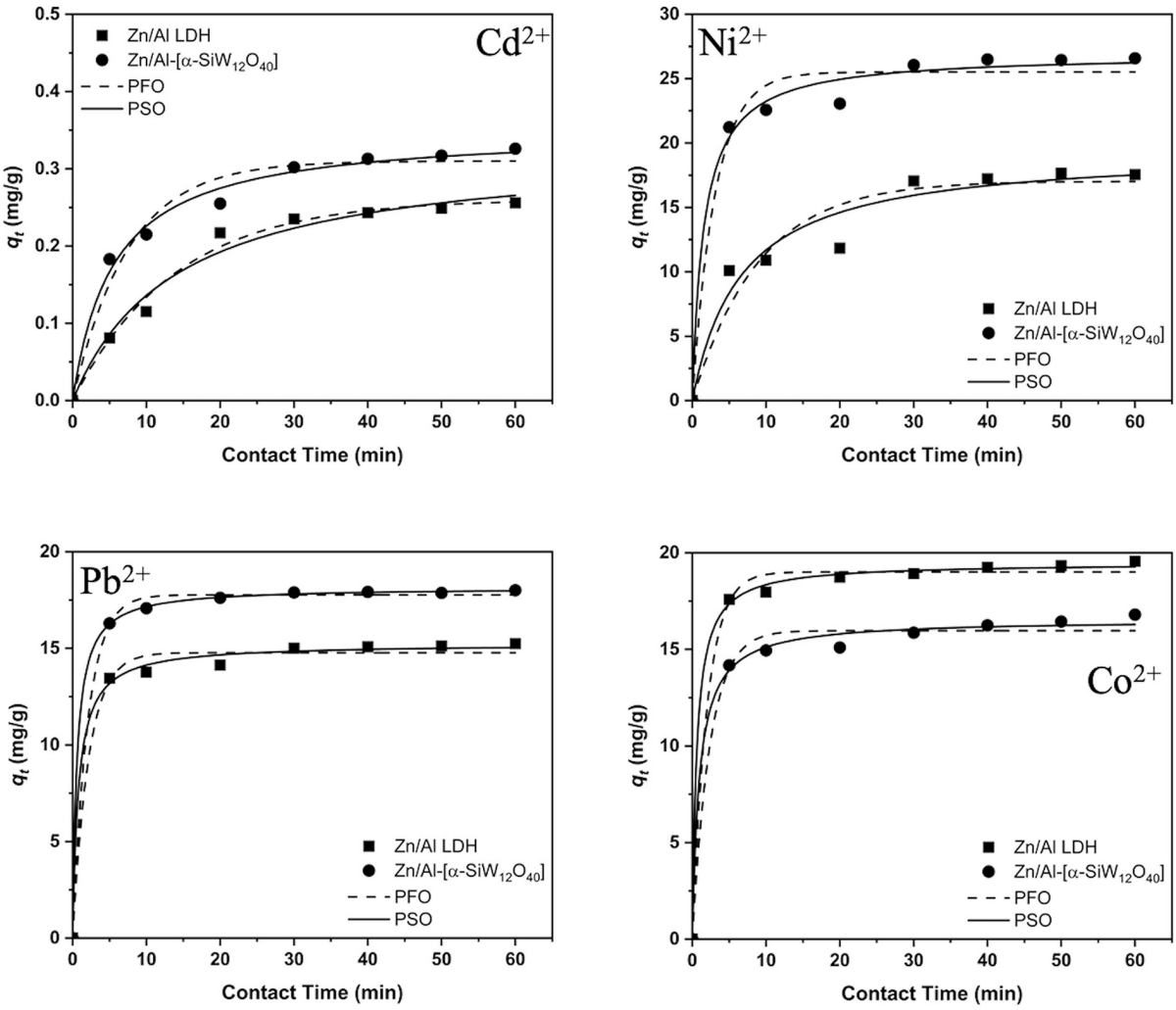

Figure 6. Effect of adsorption time of Cd^{2+}, Pb^{2+}, Ni^{2+}, and Co^{2+}

was calculated using the pseudo-first-order (PFO) and pseudo-second-order (PSO) equations. The adsorption process using Zn/Al LDHs and Zn/Al-POM is more likely to follow the PSO kinetic model with a correlation coefficient (R^2) close to 1 [Siregar et al., 2021].

The data in Table 5 shows that the adsorption of Cd^{2+}, Pb^{2+}, Ni^{2+}, and Co^{2+} on Zn/Al LDHs and Zn/Al-POM with k_2 values for Zn/Al LDHs is lower than Zn/Al-POM; this indicates that the reactivity of Zn/Al is smaller than that of Zn/Al-POM. Thus, Table 5 also shows the Zn/Al-POM has a higher adsorbed concentration than Zn/Al LDHs.

The ability of Zn/Al LDHs and Zn/Al-POM adsorbents in overcoming the Cd^{2+}, Pb^{2+}, Ni^{2+}, and Co^{2+} contamination were also tested by the regeneration process. Regeneration is carried out to determine the effectiveness of the adsorbent in reusability. Before regeneration is carried out, the first thing to determine is the desorption solvent. The desorption process Co^{2+}, Cd^{2+}, Ni^{2+}, and Pb^{2+} uses several reagents such as water, hot water, hydrochloric acid, and sodium hydroxide which are presented in Figure 7.

Overall, the desorption process of Cd^{2+}, Pb^{2+}, Ni^{2+}, and Co^{2+} showed the highest percentage of hydrochloric acid. The use of hydrochloric acid in the desorption of Pb^{2+} using Zn/Al LDHs even reached 100%. On the basis of these data, it has been confirmed that hydrochloric acid is capable of being an effective desorption solvent for Cd^{2+}, Pb^{2+}, Ni^{2+}, and Co^{2+}. Furthermore, hydrochloric acid was used as a desorption solvent for the regeneration process, the results of which can be seen in Figure 8.

The results of Cd^{2+} regeneration in Figure R(a) show that the use of Zn/Al LDHs decreased from 24.50 to 3.56%. Modified Zn/Al-POM showed decreasing stability from 44.74%

Table 5. Kinetic adsorption model for removal of Cd^{2+}, Pb^{2+}, Ni^{2+}, and Co^{2+}

Metals	Kinetic Model	Parameter	Zn/Al	Zn/Al-POM
Cd^{2+}	PFO	$Qe_{experiment}$ (mg/g)	0.276	0.354
		Qe_{calc} (mg/g)	4.745	3.882
		k_1 (min^{-1})	0.027	0.002
		R^2	0.892	0.715
	PSO	$Qe_{experiment}$ (mg/g)	0.276	0.354
		Qe_{calc} (mg/g)	0.283	0.351
		k_2 (g/mg.min)	0.002	0.007
		R^2	0.996	0.996
Ni^{2+}	PFO	$Qe_{experiment}$ (mg/g)	17.551	26.585
		Qe_{calc} (mg/g)	17.556	15.282
		k_1 (min^{-1})	0.009	0.105
		R^2	0.905	0.922
	PSO	$Qe_{experiment}$ (mg/g)	17.551	26.585
		Qe_{calc} (mg/g)	20.120	27.624
		k_2 (g/mg.min)	0.006	0.015
		R^2	0.978	0.998
Pb^{2+}	PFO	$Qe_{experiment}$ (mg/g)	15.239	18.012
		Qe_{calc} (mg/g)	2.768	2.316
		k_1 (min^{-1})	0.067	0.087
		R^2	0.935	0.969
	PSO	$Qe_{experiment}$ (mg/g)	15.239	18.012
		Qe_{calc} (mg/g)	15.527	18.148
		k_2 (g/mg.min)	0.052	0.093
		R^2	0.999	0.999
Co^{2+}	PFO	$Qe_{experiment}$ (mg/g)	16.797	19.556
		Qe_{calc} (mg/g)	3.314	2.464
		k_1 (min^{-1})	0.043	0.049
		R^2	0.9767	0.9866
	PSO	$Qe_{experiment}$ (mg/g)	16.797	19.556
		Qe_{calc} (mg/g)	17.064	19.762
		k_2 (g/mg.min)	0.033	0.052
		R^2	0.999	0.999

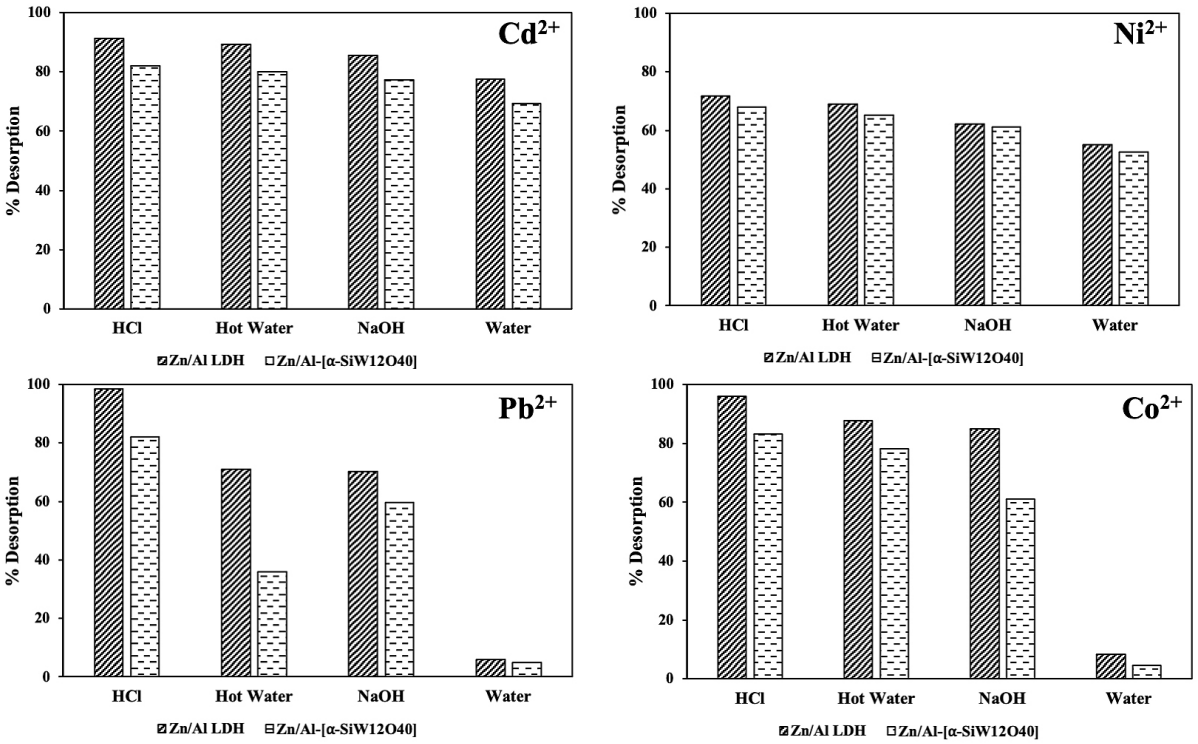

Figure 7. Desorption Cd^{2+}, Pb^{2+}, Ni^{2+}, and Co^{2+} from Zn/Al LDHs and Zn/Al-POM

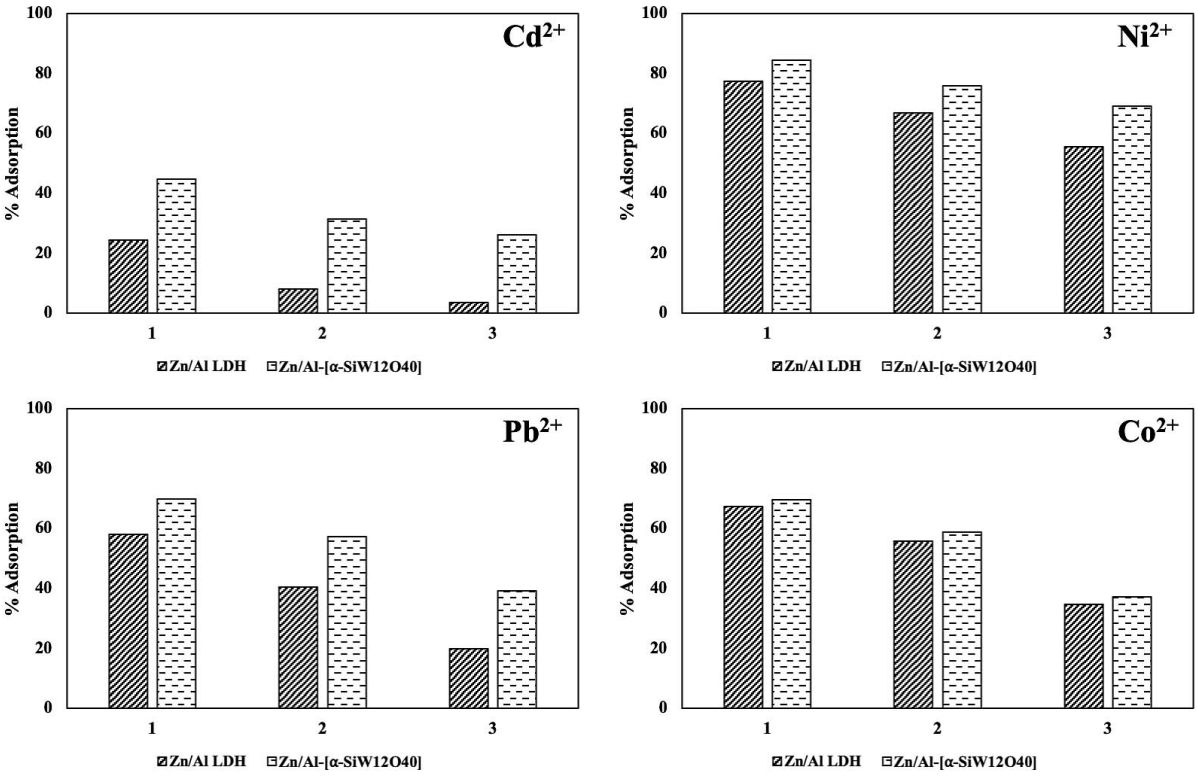

Figure 8. Zn/Al LDHs and Zn/Al-POM adsorbent regeneration ability

to 26.10% compared to Zn/Al LDHs. The Ni^{2+} regeneration process showed the highest value of 77.33% in Zn/Al LDHs and 84.52% in Zn/Al-POM in the first cycle. The last cycle showed a decrease that reached 55.52% in Zn/Al LDHs and 69.19% in Zn/Al-POM.

CONCLUSIONS

Modification of Zn/Al LDHs to Zn/Al-POM has been successful. This is proven by the XRD characterization data which shows an increase in interlayer distance from 8.59 Å to 10.26 Å, and supporting data from FT-IR, and BET. The ability of Zn/Al-POM in the adsorption process is indicated by the Qmax value of each 0.98, 55.56, 74.13, and, 43.86 mg/g; this proves that there is a match between the HSAB theory and the order of adsorption capacity of Pb^{2+}>Ni^{2+}>Co^{2+}>Cd^{2+}. Adsorption of Cd^{2+} has the smallest Qmax value, compared to Pb Cd^{2+}, Ni Cd^{2+} and Co Cd^{2+}, this supports the HSAB theory where Cd^{2+} is soft while adsorbents (LDHs) which are hard make the interactions that occur tend to be weak, causing lower adsorption capacity. The ability of Zn/Al-POM in the adsorption process was proven by the Qmax value which reached 74.13 mg/g on Pb^{2+} adsorption. In addition, the ability of Zn/Al-POM was also proven by the regeneration process which lasted up to 69.19% in the last cycle of Ni^{2+} adsorption.

Acknowledgements

Authors thank the Ministry of Education and Culture, Republik Indonesia for financial support of this research through "HIBAH DISERTASI DOKTOR" 2020–2021 from Directorate General Higher Edication (DIKTI) Republic Indonesia with primary contract number: 054/E4.1/AK.04. PT/2021 and derivative contract number: 0163. 01/UN9. SB3.LP2M.PT/2021. Special thanks to the Laboratory of research of inorganic materials and complexes, Faculty of Mathematics and Natural Sciences, Sriwijaya University.

REFERENCES

1. Alfarra A., Frackowiak E., Béguin F. 2004. The HSAB concept as a means to interpret the adsorption of metal ions onto activated carbons. Applied Surface Science, 228(1–4), 84–92.
2. Ali I., Asim M., Khan T.A. 2012. Low cost adsorbents for the removal of organic pollutants from wastewater. Journal of Environmental Management, 113, 170–183.
3. Cai P., Zheng H., Wang C., Ma H., Hu J., Pu Y., Liang P. 2012. Competitive adsorption characteristics of fluoride and phosphate on calcined Mg-Al-CO_3 layered double hydroxides. Journal of Hazardous Materials, 213–214, 100–108.
4. Castro-Castro J.D., Macías-Quiroga I.F., Giraldo-Gómez G.I., Sanabria-González N.R. 2020. Adsorption of Cr(VI) in Aqueous Solution Using a Surfactant-Modified Bentonite. Scientific World Journal, 17, 1–11.
5. Chai J.B., Au P.I., Mubarak N.M., Khalid M., Ng W.P.Q., Jagadish P., Walvekar R., Abdullah E.C. 2020. Adsorption of heavy metal from industrial wastewater onto low-cost Malaysian kaolin clay–based adsorbent. Environmental Science and Pollution Research, 27(12), 13949–13962.
6. Chakraborty R., Asthana A., Singh A.K., Jain B., Susan A.B.H. 2020. Adsorption of heavy metal ions by various low-cost adsorbents: a review. International Journal of Environmental Analytical Chemistry, 1–38.
7. Chen C. & Wang X. 2006. Adsorption of Ni(II) from aqueous solution using oxidized multiwall carbon nanotubes. Industrial and Engineering Chemistry Research, 45(26), 9144–9149.
8. Cocheci L., Barvinschi P., Pode R., Seftel E.M., Popovici E. 2010. Chromium(VI) ion removal from aqueous solutions using a Zn-Al-type layered double hydroxide. Adsorption Science and Technology, 28(3), 267–279.
9. Forghani M., Azizi A., Livani M.J., Kafshgari L.A. 2020. Adsorption of lead(II) and chromium(VI) from aqueous environment onto metal-organic framework MIL-100(Fe): Synthesis, kinetics, equilibrium and thermodynamics. Journal of Solid State Chemistry, 291, 121636.
10. Hamisu A.M., Ariffin A., Wibowo A.C. 2020. Cation exchange in metal-organic frameworks (MOFs): The hard-soft acid-base (HSAB) principle appraisal. Inorganica Chimica Acta, 511, 119801.
11. Hoyos-Sánchez M.C., Córdoba-Pacheco A.C., Rodríguez-Herrera L.F., Uribe-Kaffure R. 2017. Removal of Cd (II) from aqueous media by adsorption onto chemically and thermally treated rice husk. Journal of Chemistry, 2017.
12. Juleanti N., Palapa N.R., Taher T., Hidayati N., Putri B.I., Lesbani A. 2021. The capability of biochar-based CaAl and MgAl composite materials as adsorbent for removal Cr (VI) in aqueous solution. Science and Technology Indonesia, 6(3), 196-203.
13. Kushwaha A.K., Gupta N., Chattopadhyaya M.C. 2017. Dynamics of adsorption of Ni(II), Co(II) and Cu(II) from aqueous solution onto newly synthesized poly[N-(4-[4-(aminophenyl)methylphenylmethacrylamide])]. Arabian Journal of Chemistry, 10(2), 1645–1653.
14. Lesbani A., Normah N., Palapa N.R., Taher T., Andreas R., Mohadi R. 2020. Removal of iron(II) using Ni/Al layered double hydroxide intercalated with keggin ion. MOLEKUL, 15(3), 149–157.
15. Lin S.T., Tran H.N., Chao H.P., Lee J.F. 2018. Layered double hydroxides intercalated with sulfur-containing organic solutes for efficient removal of cationic and oxyanionic metal ions. Applied Clay Science, 162, 443–453.
16. Mamat M., Abdullah M.A.A., Kadir M.A., Jaafar A.M., Kusrini E. 2018. Preparation of layered double hydroxides with different divalent metals for the adsorption of methyl orange dye from aqueous solutions. International Journal of Technology, 9(6), 1103–1111.

17. Marques B.S., Dalmagro K., Moreira K.S., Oliveira M.L.S., Jahn S.L., de Lima Burgo T.A., Dotto G.L. 2020. Ca–Al, Ni–Al and Zn–Al LDH powders as efficient materials to treat synthetic effluents containing o-nitrophenol. Journal of Alloys and Compounds, 838(2020), 155628.
18. Mohamed E., Kamal E., Doha B., Samira S., Abdessalem T. 2019. Adsorption thermodynamics and isosteric heat of adsorption of Thymol onto sodic, pillared and organic bentonite. Mediterranean Journal of Chemistry, 8(6), 494–504.
19. Moller M. & Pich A. 2017. Development of Modified Layered Silicates with Superior Adsorption Properties for Uptake of Pollutants from Air and Water. Development of Modified Layered Silicates with Superior Adsorption Properties for Uptake of Pollutants from Air and Water Von.
20. Moyo M., Chikazaza L., Nyamunda B.C., Guyo U. 2013. Adsorption batch studies on the removal of Pb(II) using maize tassel based activated carbon. Journal of Chemistry, 2013.
21. Normah N., Palapa N.R., Taher T., Mohadi R., Utami H.P., Lesbani A. 2021. The Ability of composite Ni/Al-carbon based material toward readsorption of iron (II) in aqueous solution. Science and Technology Indonesia, 6(3), 156-165
22. Oktriyanti M., Palapa N.R., Mohadi R., Lesbani A. 2020. Effective removal of iron (II) from aqueous solution by adsorption using Zn/Cr layered double hydroxides intercalated with Keggin ion. Journal of Ecological Engineering, 21(5), 63–71.
23. Onder A., Ilgin P., Ozay H., Ozay O. 2020. Removal of dye from aqueous medium with pH-sensitive poly[(2-(acryloyloxy)ethyl]trimethylammonium chloride-co-1-vinyl-2-pyrrolidone] cationic hydrogel. Journal of Environmental Chemical Engineering, 8(5), 104436.
24. Palapa N.R., Juleanti N., Mohadi R., Taher T., Rachmat A. 2020. Copper aluminum layered double hydroxide modified by biochar and its application as an adsorbent for procion red. Journal of Water and Environment Technology, 18(6), 359–371.
25. Palapa N.R., Taher T., Mohadi R., Rachmat A., Mardiyanto M., Miksusanti M. & Lesbani A. 2021a. NiAl-layered double hydroxide intercalated with Keggin polyoxometalate as adsorbent of malachite green: kinetic and equilibrium studies, Chemical Engineering Communications, DOI: 10.1080/00986445.2021.1895773.
26. Palapa N.R., Taher T., Wijaya A., Lesbani A. 2021b. Modification of Cu/Cr layered double hydroxide by keggin type polyoxometalate as adsorbent of malachite green from aqueous solution. Science and Technology Indonesia, 6(3), 156-165
27. Silaen L., Rahayu N., Mohadi R., Lesbani A. 2021. Intercalated Zn-Cr-[α-SiW12O40] as Removal Agents of Cobalt (II) in Watery Phase: Adsorption and Regeneration Stud. Chiang Mai J.Sci., 48(2), 545–556.
28. Siregar P.M.S.B.N., Palapa N.R., Wijaya A., Fitri E.S., Lesbani A. 2021. Structural Stability of Ni/Al Layered Double Hydroxide Supported on Graphite and Biochar Toward Adorption of Congo Red. Science and Technology Indonesia, 6(2), 85–95.
29. Taher T., Christina M.M., Said M., Hidayati N., Ferlinahayati F., Lesbani A. 2019a. Removal of iron(II) using intercalated Ca/Al layered double hydroxides with [-SiW12O40]4-. Bulletin of Chemical Reaction Engineering & Catalysis, 14(2), 260–267.
30. Taher T., Irianty Y., Mohadi R., Said M., Andreas R., Lesbani A. 2019b. Adsorption of cadmium(Ii) using ca/al layered double hydroxides intercalated with keggin ion. Indonesian Journal of Chemistry, 19(4), 873–881.
31. Taher T., Rohendi D., Mohadi R., Lesbani A. 2019c. Congo red dye removal from aqueous solution by acid-activated bentonite from sarolangun: kinetic, equilibrium, and thermodynamic studies. Arab Journal of Basic and Applied Sciences, 26(1), 125–136.
32. Taiwo A.F. & Chinyere N.J. 2016. Sorption characteristics for multiple adsorption of heavy metal ions using activated carbon from Nigerian bamboo. Journal of Materials Science and Chemical Engineering, 4(4), 39–48.
33. Tang Z., Qiu Z., Lu S., Shi X. 2020. Functionalized layered double hydroxide applied to heavy metal ions absorption: A review. Nanotechnology Reviews, 9(1), 800–819.
34. Tchounwou P.B., Yedjou C.G., Patlolla A.K., Sutton D.J. 2012. Molecular, clinical and environmental toxicicology. Environmental Toxicology, 3, 133–164.
35. Wahab N., Saeed M., Ibrahim M., Munir A., Saleem M., Zahra M., Waseem A. 2019. Synthesis, characterization, and applications of silk/bentonite clay composite for heavy metal removal from aqueous solution. Frontiers in Chemistry, 7, 1–12.
36. Wang X., Cui Y., Peng Q., Fan C., Zhang Z., Zhang X. 2020. Removal of Cd(II) and Cu(II) from aqueous solution by Na+-modified pisha sandstone. Journal of Chemistry, 2020.
37. Wang Y. & Zhang L. 2020. Improved performance of 3D hierarchical NiAl-LDHs micro-flowers via a surface anchored ZIF-8 for rapid multiple-pollutants simultaneous removal and residues monitoring. Journal of Hazardous Materials, 395, 122635.
38. Zhang Y.X., Hao X.D., Kuang M., Zhao H., Wen Z.Q. 2013. Preparation, characterization and dye adsorption of Au nanoparticles/ZnAl layered double oxides nanocomposites. Applied Surface Science, 283, 505–512.
39. Zhang X., Yan L., Li J., Yu H. 2020. Adsorption of heavy metals by L-cysteine intercalated layered double hydroxide: Kinetic, isothermal and mechanistic studies. Journal of Colloid and Interface Science, 562, 149–158.
40. Zhang T., Zhao B., Chen Q., Peng X., Yang D., Qiu F. 2019. Layered double hydroxide functionalized biomass carbon fiber for highly efficient and recyclable fluoride adsorption. Applied Biological Chemistry, 62(1), 1–7.
41. Zhao Y., Zhan L., Xue Z., Yusef K.K., Hu H., Wu M. 2020. Adsorption of Cu (II) and Cd (II) from wastewater by sodium alginate modified materials. Journal of Chemistry, 2020.